Structure of the Stretching Field in Chaotic Cavity Flows

M. Liu and R. L. Peskin
Dept. of Mechanical Engineering

F. J. Muzzio
Dept. of Chemical and Biochemical Engineering
Rutgers University, Piscataway, NJ 08855

C. W. Leong
Raychem Corporation, Process Technology Group, Menlo Park, CA 94025

Stretching of material elements in time-periodic cavity flows is investigated numerically. The spatial structure of the stretching field is determined not only by nonchaotic islands and by unstable manifolds of hyperbolic periodic points, but also by singularities of the flow field at the cavity corners. For the short time scales interesting to most mixing applications, regions of very high stretching (good local mixing) are determined by unstable manifolds that pass close to the corners of the cavity. Low stretching (poor local mixing) regions are usually found both inside and near islands. In some cases, however, the unstable manifolds wrap themselves around the islands, preventing the formation of segregated low stretching subregions within the chaotic region.

Introduction

Mixing is essential to many processes in nature and in technology. Applications span wide ranges of time and length scales; extreme cases are the earth mantle, whose evolution is governed by motions that occur over thousands of years and produce structures that are measured in kilometers, and turbulent reactive flows, which are controlled by flow fluctuations that last a few microseconds and act over length scales of a few microns. The industrial importance of mixing can hardly be exaggerated. Chemical processes often require using a mixing flow to bring reactants into intimate contact. If reactions are fast or the medium is viscous, significant reaction occurs before mixing is completed, often causing poor product quality, need for large and complicated separation stages, excessive pollution, and in general resulting in adverse economics.

Important advances in the study of fluid mechanical mixing have been facilitated by experiments and simulations of convection of passive tracers in laminar flows, leading to numerous observations (Khakhar et al., 1986; Aref and Balachandar, 1986; Chien et al., 1986; Chaiken et al., 1986; Ottino et al., 1988; Leong and Ottino, 1989; Rom-Kedar et al., 1990; Swanson and Ottino, 1990). However, a comprehensive framework capable of quantifying mixing effects is missing. The development of such a framework is a daunting task. Part of the problem is semantic; the current terminology contains many loosely defined terms (mixing, stirring, blending, convection, advection, diffusion, and so on) referring to a number of related effects. The main difficulty, however, stems from the nature of mixing itself. The best fluid mechanical mixing is produced by flows that redistribute material elements throughout space in a random-like manner, producing partially mixed spatial structures composed of regions of distributed sizes in which different components predominate. Therefore, randomness is a desirable phenomenon, which is usually achieved by using either a turbulent or a chaotic flow to produce the mixing. However, it is common to observe elements of order coexisting with the randomness, such as coherent structures in turbulent flows, and symmetries and nonchaotic regions in chaotic flows.

Understanding these combinations of order and randomness is crucial to the comprehension of the mixing process and constitutes the main challenge in the analysis. On one hand, if the particles follow random trajectories, the equations of

Correspondence concerning this article should be addressed to F. J. Muzzio.

motion cannot be integrated in closed form, greatly restricting predicting capabilities. On the other hand, purely statistical methods are poorly suited for the analysis of situations where large degrees of order are present. Progress can be made by focusing on flows where both order and randomness are present in controllable and reproducible ways. Time periodic chaotic flows are ideal models for this purpose. Chaotic motion can be generated by using simple velocity fields that are easy to simulate and that in some cases admit experimental implementation. The flows often show a mixture of chaotic and nonchaotic regions, and the size of regions of each kind can be controlled accurately by fine-tuning flow parameters.

In principle, an experimental approach for quantifying mixing, based on measurements of the distribution of length scales observed in partially mixed structures, is possible (Dahm et al., 1991). However, such measurements are subject to parallax and fluorescence errors that are of the same order of magnitude as the striation thicknesses themselves (Leong and Ottino, 1989). Fortunately, computations of the stretching field in model flows can provide extensive descriptions of both the dynamics and spatial structure of the mixing process. Analysis of stretching in time-periodic chaotic flows has attracted considerable attention in recent years and is increasingly becoming something of a standard tool for both qualitative and quantitative characterization of fluid mechanical mixing in these systems. The analysis is by no means limited to time-periodic chaotic flows; in fact, it can be applied to any flow where particle trajectories can be computed. Unfortunately, these ideas have not been presented in organized fashion to the engineering community, which is best suited to develop practical applications. One of the goals of this article is to fill this gap in the literature. The main concepts involved in using stretching computations for analyzing fluid mechanical mixing are discussed, along with a brief review of the recent literature. These concepts are illustrated by a realistic example, the cavity flow system. The flow and numerical algorithms are presented, as well as computations of the stretching field along the trajectories of point particles (a Hamiltonian system). Statistical analysis of stretching is presented before final conclusions.

Stretching in Chaotic Flows

Recent work has shown that the evolution of partially mixed structures can be specified by computing the deformation (stretching) and position (stirring) of a population of material elements scattered throughout the system (Rom-Kedar et al., 1990; Pierrehumbert, 1991; Muzzio et al., 1991a, 1992a,b; Városi et al., 1991; Beigie et al., 1991, 1993; Wiggins, 1992). Stretching and stirring are both important. Since the amount of intermaterial surface created in a given region of a flow is directly proportional to the amount of stretching experienced by material elements in the region, the rate of stretching determines the local rate of the mixing process (the rate of micromixing). Stirring, on the other hand, relocates material elements, spreading them throughout space, and determines the degree of spatial uniformity (macromixing).

Computations of stretching provide the means for characterizing distributions of mixing intensities commonly observed in practical applications. The positions of points experiencing high and low stretching respectively determine regions of good and bad micromixing. The local average stretching at final positions can be used to estimate the value at those positions of material properties that depend on the degree of intermingling and to determine the optimal location of injection ports for industrial mixing applications. Statistical quantities, such as the probability density function of stretching values, make it possible to compare mixing in different flows or in the same flow at different times. Moreover, stretching of material elements has immediate implications for other phenomena of practical importance, such as diffusive transport (Aref and Jones, 1988; Jones, 1991; Wiggins, 1992); chemical reactions (Ottino, 1982; Muzzio and Ottino, 1989a,b, 1990), and drop breakup (Muzzio et al., 1991b; Tjahjadi et al., 1992).

Several recent studies have focused on distributions of finite-time Lyapunov exponents. These exponents are immediately related to stretching (the finite-time Lyapunov exponent is simply the logarithm of stretching divided by time). Grassberger et al. (1988) introduced the spectrum of finite-time Lyapunov exponents and computed results for the logistic map and for Henon's map. Sepulveda et al. (1989) focused on the standard map for a condition with large nonchaotic regions. Their results showed that while chaotic regions generated a nearly time-invariant spectrum, nonchaotic regions (islands) generated spectra that were strongly time-dependent. These results were expanded by Horita et al. (1990), who also used the standard map but focused on conditions for which the map was chaotic everywhere or had only small islands. For globally chaotic conditions, the map generated a nearly self-similar spectrum for the full range of Lyapunov exponents. Nearly Gaussian self-similar spectra were also reported by Városi et al. (1991) for a *randomized* standard map. Pierrehumbert (1991), in a recent study, calculated the structure and statistics of finite-time Lyapunov exponents for atmospheric flow in the northern hemisphere. Results were in good qualitative agreement with similar calculations for the idealized standard map mentioned above. Finally, Beigie et al. (1993) recently computed distributions of finite-time Lyapunov exponents along the unstable manifolds of perturbed heteroclinic tangles. They found that depending on flow conditions, Lyapunov exponents were well described by either a Gaussian or an exponential distribution.

These studies have made clear that a great deal of universality is present in the dynamics of finite-time Lyapunov exponents in chaotic systems. However, most of the studies mentioned above have focused on highly idealized maps with unclear physical counterparts [the main exception is the study by Pierrehumbert (1991)]. To develop practical mixing applications, it is important to determine whether realistic flow systems exhibit the same types of behavior. To keep the discussion in practical terms, we focus on stretching rather than on Lyapunov exponents. To this date, the stretching field has been investigated for only one physically realizable system, that is, the flow between eccentric cylinders (Aref, 1984; Aref and Jones, 1988; Swanson and Ottino, 1989). Muzzio et al. (1991a, 1992a,b) analyzed both the structure and the statistics of stretching in this flow. Stretching was distributed in highly nonuniform fashion. Regions of high stretching were generated by the unstable manifolds of periodic hyperbolic points. Similarly to the standard map (Sepulveda et al., 1989; Horita et al., 1990), regions of low stretching were found both inside islands and attached to islands. Additional low stretching regions, caused by the presence of solid walls at the system

boundaries, were unavoidable even for "globally chaotic" conditions.

These observations have practical implications for mixing. Flows that simultaneously exhibit regions of very high and very low stretching generate partially mixed structures with extremely nonuniform degrees of local mixedness. In flows with segregated high stretching regions, material elements have a finite, nonvanishing probability of experiencing extremely large stretching rates, possibly resulting in damage of shear sensitive material or in hot spots for transport-controlled exothermic reactions (such effects are sometimes observed in extruder flows). The presence of persistent low stretching regions means that there are practical limitations to the efficiency of mixing that can be achieved in practice. Therefore, it is important to determine which characteristics of the stretching field are universal and which are particular attributes of specific systems. To do that, the analysis must be extended to include other cases of practical importance. This study focuses on another physically realizable case, the chaotic cavity flow (Leong and Ottino, 1989). Similarly to the flow between eccentric cylinders, the cavity flow can be studied using both experiments and computations. However, the cavity flow is very different than the flow between eccentric cylinders. For theoretical cavity flows, the four corners of the cavity are singular points where the velocity gradient is infinite; very large gradients at the corners are expected in experimental cavity flows. It is shown below that these corner effects have important effects on the structure of the stretching field. The flow between eccentric cylinders lacks such singularities and behaves very differently than the cavity.

Flow System and Algorithms

The cavity flow was chosen as a case study for several reasons. The flow has been implemented experimentally (Leong and Ottino, 1989) and data is available to assess accuracy of the simulations. The periodic cavity flow is defined in a rectangular domain with two moving walls and two stationary walls (Figure 1). A convenient dimensionless description is obtained by adopting the length of the moving horizontal walls, L, and the mean wall velocity, U, as length and velocity scales, respectively. The aspect ratio of the cavity is constant for all the results reported in this article, and the length of the stationary vertical walls is $0.6L$. Chaos is generated by alternatively moving the top and bottom walls with constant velocity each for a time $T/2$, where T, the nondimensional period of the flow, is defined as the total combined displacement of both walls during one period, divided by the length of the cavity. The behavior of the system depends strongly on the period T (Leong and Ottino, 1989). While at low values of $T \approx 1.0$, particles move regularly for all initial positions, for most values of T between 3 and 13, both regular and chaotic particle trajectories exist in the flow (Liu, 1992).

The equations governing the theoretical flow are the mass and momentum balances, which in dimensionless form for incompressible and isothermal Newtonian fluids are:

$$\nabla \cdot v = 0, \tag{1a}$$

$$\partial v/\partial t + v \cdot \nabla v = -\nabla p + (1/Re)\nabla^2 v \tag{1b}$$

where p is the dimensionless pressure and Re is the Reynolds number. In principle, for this unsteady flow v must be obtained by solving Eqs. 1a and 1b numerically with appropriate boundary conditions. The trajectories of fluid particles are then computed by integrating the velocity field. However, in order to compute a statistically significant distribution of stretching values, a large number of particles must be used. Each such computation would in principle require a very large amount of computer time, rendering our approach impractical given current computational limitations. This situation can be avoided by restricting the study to slow flows. For $Re \leq 1.0$, the nonlinear inertial term $v \cdot \nabla v$ on Eq. 1b is negligible compared to the viscous term $(1/Re)\nabla^2 v$ (for details see Liu, 1992). This has two consequences: the equation of motion (Eq. 1b) is linear in v, and changes in the motion of the wall are transmitted throughout the flow nearly instantaneously, and therefore, each time the upper wall stops and the lower one is set in motion (or vice versa), the velocity field throughout the rectangular domain can be assumed to switch instantaneously from the steady flow produced by the motion of the upper wall to the steady flow produced by the motion of the lower wall. This assumption is supported by experimental evidence provided by Leong (1990), who showed that the slow unsteady flow was reversible, and therefore, that the transients that occur when a wall is stopped and the other is set in motion are negligible. Therefore, for low Reynolds numbers, once the *steady* cavity flow field is obtained, no additional computation of the velocity field is required. The periodic cavity flow can be simulated by switching on and off two steady cavity flows that are mirror images of one another (streamlines for these two flows are displayed in Figure 1), and particle trajectories can be integrated. This procedure greatly reduces the computer time required to obtain statistically significant distributions of stretching values.

In this study, v and ∇v are obtained numerically for a grid of (100×100) nodal points using a second-order finite difference method to solve the vorticity and stream function equations derived from Eq. 1. The amount of stretching experienced by a material segment passively convected by a flow is deter-

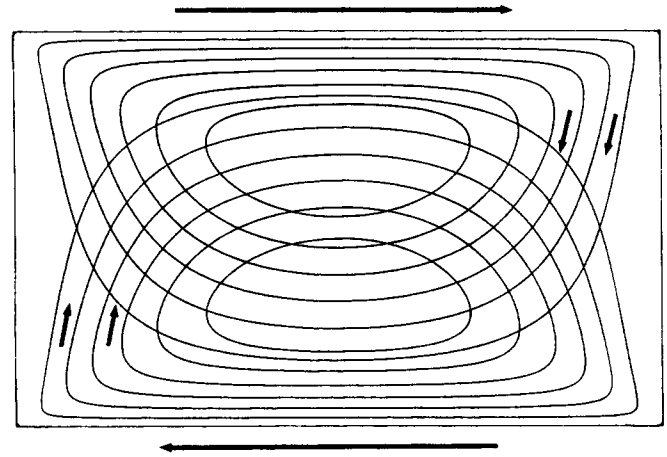

Figure 1. Idealized cavity flow is produced by moving the top and/or the bottom wall while keeping the vertical walls stationary.

Sketch represents a steady co-rotating flow with arrows pointing in direction of wall motion. Streamlines corresponding to separate motion of each wall are also shown.

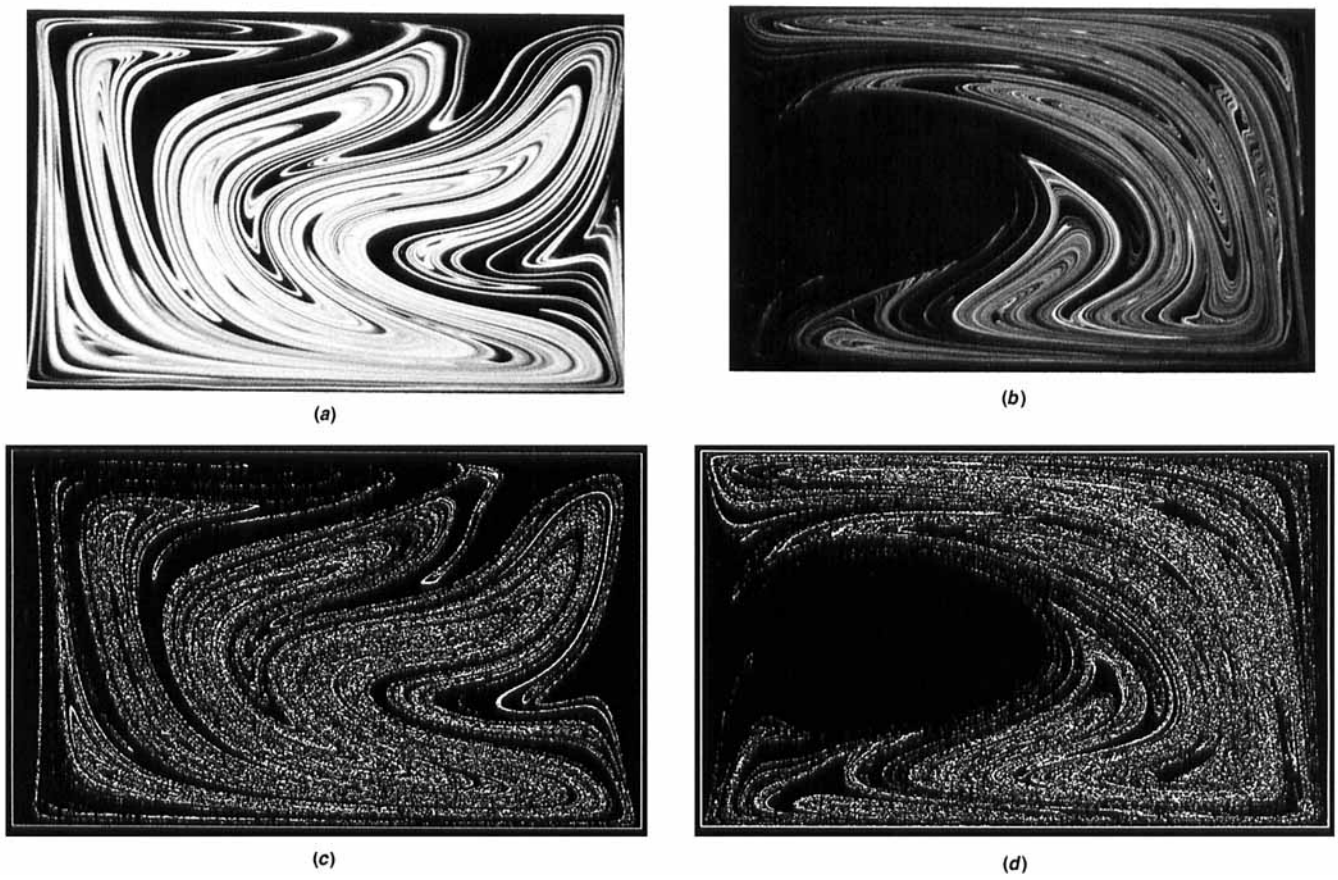

Figure 2. Comparisons of experimental and numerical results for co-rotating periodic cavity flows.

Experiments show final position of fluorescent dye tracer for (a) $T=5.6$, 10.25 periods and (b) $T=7.0$, 7 periods. Numerical simulations show final positions of 40,000 particles initially located at approximately same position of dye in experiments, for (c) $T=5.6$ and (d) $T=7.0$, same number of periods as in experiments.

mined by tracking the position x and length $|l|$ of an infinitesimal vector l whose evolution is given by:

$$dx/dt = v, \quad x_{t=0} = X_0, \tag{2a}$$

$$dl/dt = (\nabla v)^T \cdot l, \quad l_{t=0} = l_0. \tag{2b}$$

To obtain particle trajectories, v is interpolated using a fourth-order biquadratic scheme and integrated by means of a fourth-order Runge-Kutta algorithm.

The accuracy of the numerical algorithm can be assessed by comparing experimental and computational results. Figures 2a and 2b show mixing experiments (Leong and Ottino, 1989; Leong, 1990) where a passive fluorescent tracer is mixed for about ten periods of the flow for $T=5.6$ and 7.0. A convoluted structure, occupying most of the chaotic region and composed of thousands of striations with distributed thicknesses, is displayed in each case. The main features of these structures (such as location of the folds and orientation of the striations) are independent of both time and initial conditions. Small-scale features, such as individual striations and local dye concentration, are strongly dependent on time and initial location of the dye. To some extent, these mixing experiments can be simulated simply by placing a large number of particles at approximately the same initial position that the dye occupies in an experiment, and then computing the final location of the points for the same mixing interval. Figures 2c and 2d show the simulated mixing structures for $T=5.6$ and 7.0. The computational results agree well with the experiments, demonstrating the viability of the numerical algorithm. Some differences in small-scale structures are to be expected because the experimental initial conditions cannot be matched exactly due to finite numerical accuracy. Although, in principle, this type of computation could be used as a basis to quantify the distribution of length scales produced by the mixing process, the number of points needed for an accurate description of the small-scale features is very large (10^8 or more) and requires advanced simulation techniques using parallel computations of particle positions and optimal data storage/retrieval techniques.

Spatial Structure of the Stretching Field

Computations of the stretching field offer an efficient alternative for the characterization of fluid mechanical mixing processes. The stretching λ experienced by the segment after some time is defined as:

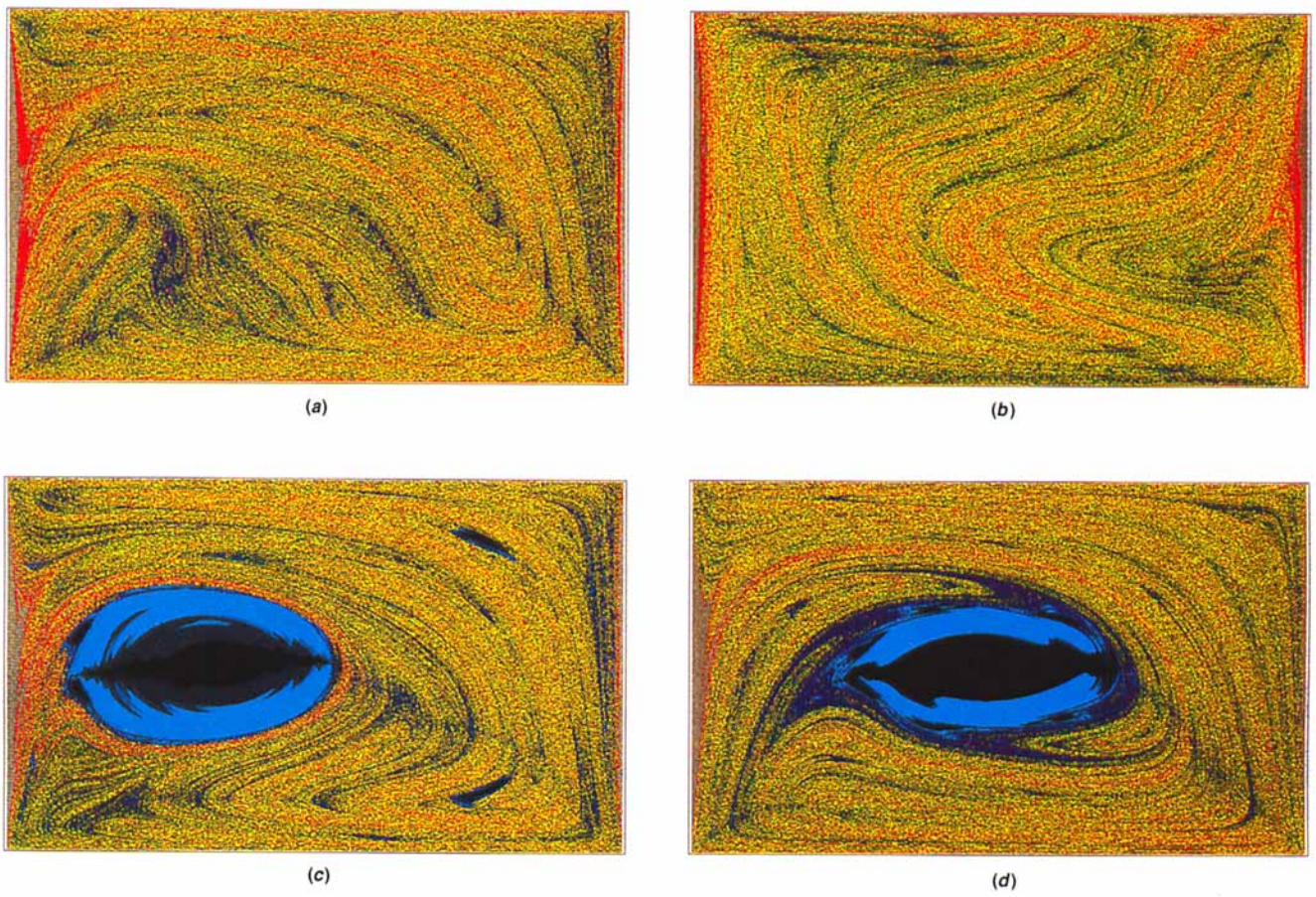

Figure 3. Particles are color-coded according to the stretching values experienced after *n* periods.

Magnitude of stretching increases in sequence of black, light blue, dark blue, green, yellow and red. Particles in black, light blue, dark blue and green have values of stretching intensities smaller than mean, and those in yellow and red have stretchings greater than mean. Colors are assigned ad hoc to enhance the graphic display of (or lack of) segregation effects (a) $T=5.6$, $n=20$, blue corresponds to $\log\lambda<6.3$, green to $6.3<\log\lambda<7.3$, yellow to $7.3<\log\lambda<8.6$, and red to $8.6<\log\lambda$; (b) same as Figure 3a but for $n=20.25$ periods; (c) $T=7.0$, $n=20$, black corresponds to $\log\lambda<1.3$, light blue to $\log\lambda<3.5$, blue to $3.5<\log\lambda<6.7$, green to $6.7<\log\lambda<8.0$, yellow to $8.0<\log\lambda<10.0$, and red to $10.0<\log\lambda$; (d) $T=9.0$, $n=12$, black corresponds to $\log\lambda<0.7$, light blue corresponds to $0.7<\log\lambda<1.8$, dark blue to $1.8<\log\lambda<6.5$, green to $6.5<\log\lambda<8.0$, yellow to $8.0<\log\lambda<9.5$, and red to $9.5<\log\lambda$.

$$\lambda = |l| / |l_0|, \tag{3}$$

with l_0 having infinitesimal length. Since vectors in chaotic regions are reoriented very rapidly in the direction of maximum stretching, the initial orientations of the vectors is largely immaterial (Pierrehumbert, 1991; Muzzio et al. 1991a, 1992a,b); computations in which the l_0 are oriented horizontally, vertically, or randomly generate identical results. Portraits of the asymptotic orientation in chaotic cavity flows have been presented by Liu (1992).

Important aspects of the spatial structure of mixing are immediately revealed by direct examination of the stretching field. The higher the value of stretching at a given position, the smaller the local striation thickness. Therefore, regions populated by points experiencing the highest and lowest stretching values respectively correspond to regions of best and worst mixing. Figure 3a shows the stretching field for $T=5.6$, 20 periods, 365,820 (780×469) points. The points are color coded according to intensity of stretching. The color sequence, from lowest to highest stretching, is black, light blue, dark blue, green, yellow, and red. Although this flow condition is globally chaotic and has an almost featureless Poincaré section (Leong, 1990; Liu, 1992), the stretching plot reveals that regions of high stretching (red) are considerably segregated. When plotted at the appropriate time, the stretching field reveals features of the partially mixed structure to a surprising degree of detail; compare Figure 3b, which shows the stretching field for $T=5.6$, 20.25 periods, with the corresponding experiment in Figure 2a. The segregation of high and low stretching regions is more intense for $T=7.0$ (Figure 3c). Again, very good agreement is observed when comparing the stretching field with a mixing experiment (Figure 2b). For this condition, points with very low stretching (black and light blue) populate a large, egg-shaped regular island to the left and the two smaller islands at symmetric positions to the right of the cavity. High stretching points (red), on the other hand, populate the chaotic region in a highly nonuniform way. The situation is considerably different for $T=9.0$ (Figure 3d). For this case, low stretching points populate both a large island at the center of the cavity as well as sharply defined regions that are attached to the island and that penetrate deeply inside the chaotic region. This results in a poorly mixed region that is roughly twice as large as the island itself. This effect would have been missed by Poincaré sections, which would have captured the island but not the

(a)

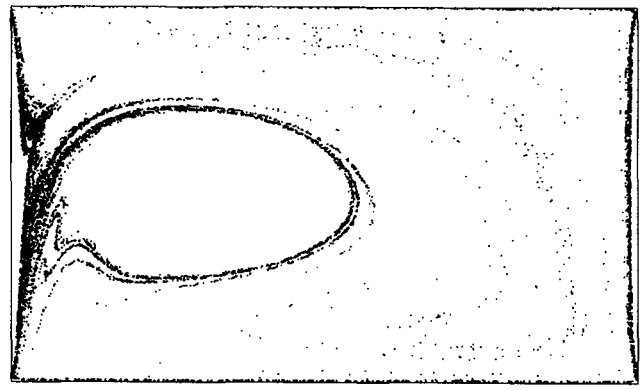

(b)

(c)

Figure 4. Spatial distribution of particles with very high stretching intensities after *n* periods.

Total number of particles in the computation is 365,820. (a) $T=5.6$, $n=10$, 8,849 particles, $\log(\lambda)>7.0$; (b) $T=7.0$, $n=10$, 7,307 particles, $\log(\lambda)>8.2$; (c) $T=9.0$, $n=12$, 13,957 particles, $\log(\lambda)>11.0$.

low stretching regions attached to it. High stretching points, on the other hand, are scattered uniformly throughout most of the chaotic region, except in the neighborhood of the island, which is devoid of such points.

High stretching regions

The stretching fields depicted in Figures 3a to 3d make it possible to gain a global appreciation of the stretching process throughout the flow. However, more details can be appreciated by separate examination of high stretching regions, shown in Figures 4a to 4c. Figure 4a shows the points with the highest stretching $\log(\lambda)>7.0$ at the end of the 10th period for $T=5.6$. Most of these points concentrate in narrow bands near the walls and in a complex structure resembling a half spiral whose arms originate at the left wall. This behavior is in sharp contrast with that observed for the flow between cylinders, which typically exhibits low stretching regions attached to walls. Figure 4b shows high stretching points corresponding to $T=7.0$, 10 periods. Once again, for this condition, many of these points concentrate near the stationary walls. The densest population of high stretching points, however, is found in a heavily populated, tight ring surrounding the largest regular island. Different behavior is displayed in Figure 4c, which shows high stretching points for $T=9.0$, 12 periods. The structure is considerably more uniform than for the previous two cases, except that the neighborhood of the island is devoid of high stretching points.

Rom-Kedar et al. (1990), Beigie et al. (1991, 1993), and Wiggins (1992) have stressed the dominant role of unstable manifolds of hyperbolic points in stretching of material lines and in mixing of passive scalars in several flows. Muzzio et al. (1992b) found that the short-time spatial organization of high stretching regions in the flow between eccentric cylinders was determined by the structure of the unstable manifolds of hyperbolic periodic points. Manifolds are invariant structures of infinite length that eventually visit every location inside a chaotic region; trajectories passing close to a hyperbolic point tend to travel along the unstable manifold for some time afterwards. In general, the lower the period of the point, the larger the influence of its manifolds. In the short times of interest for practical mixing applications, particles initially placed close to hyperbolic periodic points experience very high stretching but only reach a limited subset of the flow, giving origin to segregated high stretching regions.

However, the relationship between high stretching regions and unstable manifolds in the cavity flow, analyzed next, is considerably less straightforward. Since the cavity flow does not have fixed critical points, the analysis once again focuses on periodic points. The first step is to find the points, which is not a trivial task. A useful technique for finding odd period points, developed by Ottino and coworkers, takes advantage of the fact that periodic flows often display intantaneous symmetries. These symmetries can be found from the motion itself (Franjione et al., 1989), or by noticing that the Poincaré section becomes symmetric at discrete intervals. For example, partially mixed structures in the cavity flow become symmetric with respect to the x axis at $t=nT/2$ and with respect to the y axis at $(n/2+1/4)T$ (Leong and Ottino, 1989; Franjione et al., 1989). Odd period points are located on the axes of these symmetries, and can be found by covering the axes with a large

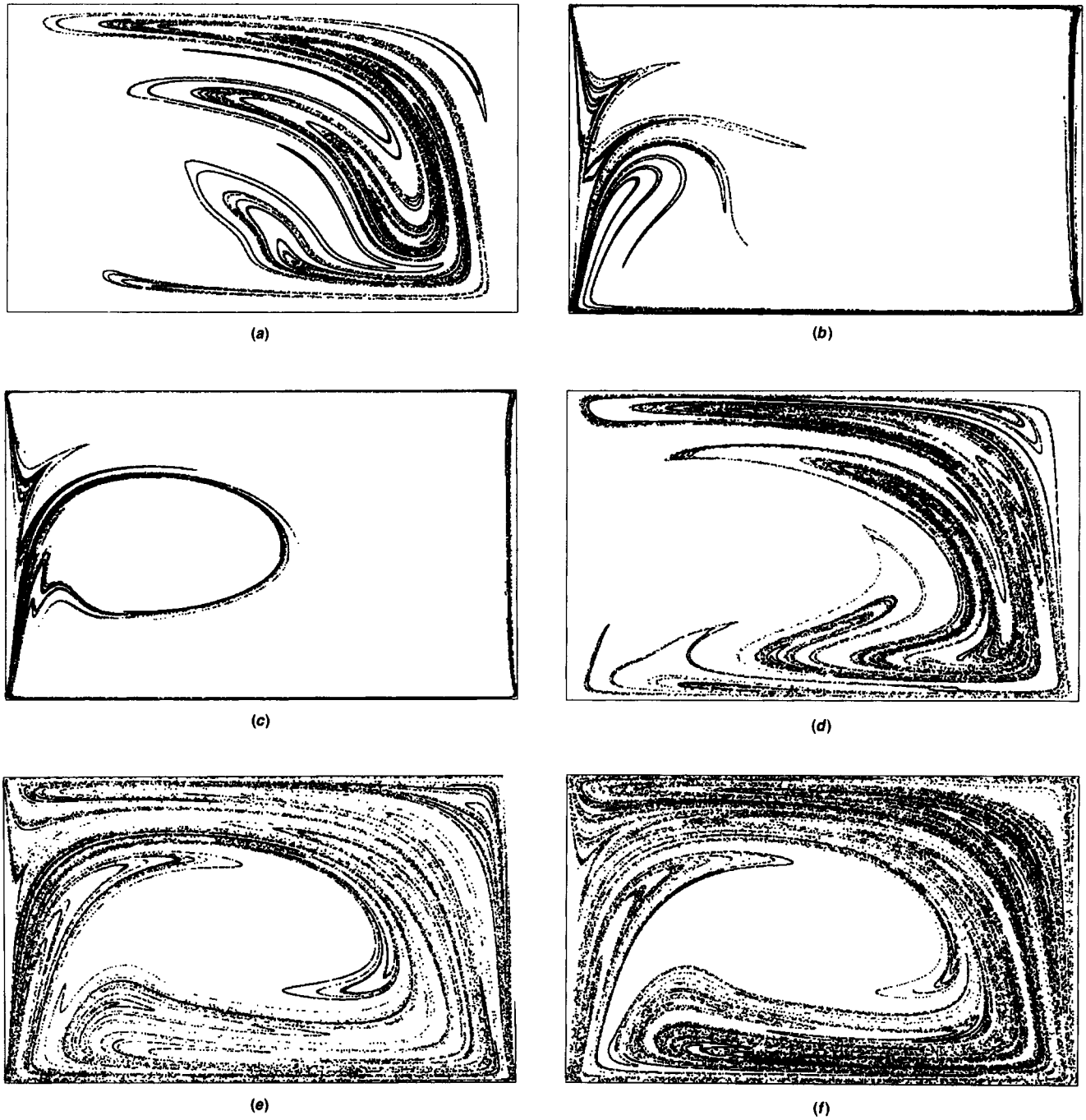

Figure 5. Unstable manifolds of hyperbolic periodic points.

In these computations, 40,000 particles were initially located in small circle centered at periodic point. Shown in figures are final positions of particles after n periods. (a) $T=5.6$, $n=6$, point initially located at $x=0.8298$; (b) $T=5.6$, $n=8$, points initially located at $x=0.0605$ and $x=0.9791$; (c) $T=7.0$, $n=5$, $x=0.0601$; (d) $T=7.0$, $n=6$, $x=0.8621$; (e) $T=9.0$, $n=4$, $x=0.03785$; (f) $T=9.0$, $n=4$, $x=0.8905$. All points are period-1 except for Figure 5b, which shows manifolds of pair of period-2 points. In all cases, points are initially located on horizontal axis $y=0.3$.

number of tracers, and identifying those tracers that return to their initial location after a given number of periods. Repetition of the procedure with increasing resolution provides an effective method for finding the points accurately (Swanson and Ottino, 1989). Even period points are usually located in pairs at symmetric positions with respect to the axes of symmetry, and are much harder to find.

Once the periodic points are located, their nature (elliptic or hyperbolic) is determined by calculating the deformation tensor, $\boldsymbol{F}$, which is computed from:

$$d\boldsymbol{F}/dt = (\nabla \boldsymbol{v})^T \cdot \boldsymbol{F}, \quad \boldsymbol{F}_{t=0} = \boldsymbol{I} \tag{4}$$

For incompressible flows such as the one considered here, if the absolute value of the trace of $\boldsymbol{F}$ is less than 2.0, the periodic point is elliptic and is surrounded by an island; if it exceeds

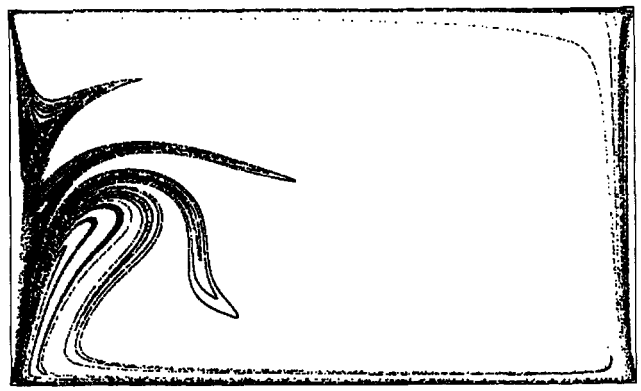

(a)

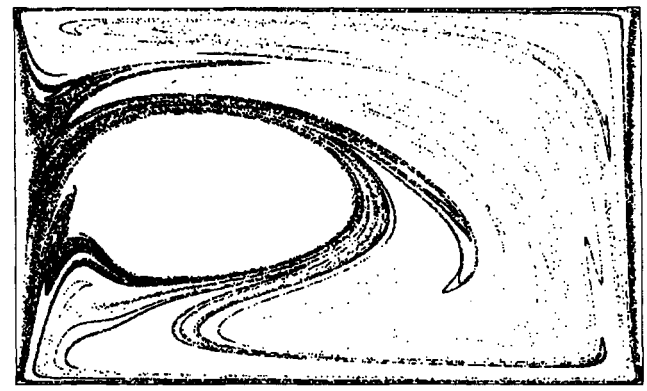

(b)

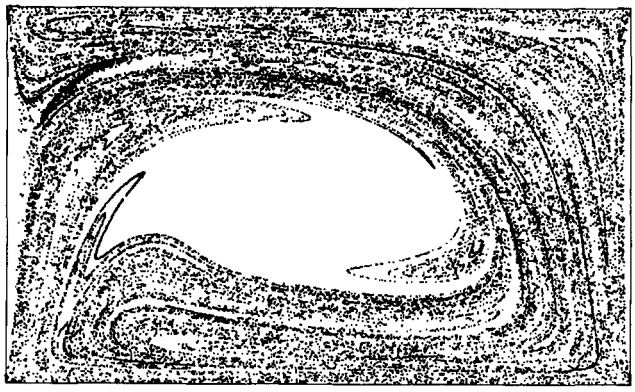

(c)

Figure 6. Final location of high stretching points initially placed at corners of cavity.

In these computations, 10,000 particles were initially located in small square near each of four corners. Shown in figures are final positions of particles after n periods. (a) $T=5.6$, $n=6$; (b) $T=7.0$, $n=6$; (c) $T=9.0$, $n=4$.

2.0, the point is hyperbolic and has stable and unstable manifolds that approach and leave the points following the eigendirections of F.

For $T=5.6$, only one period-1 hyperbolic point was found; at $t=0$, the point is on the horizontal axis at $x=0.8298$. Figure 5a shows branches of the unstable manifolds of this point that are reached by tracer particles initially placed in a small circle centered at the periodic point and then convected by the flow for 6 periods. Direct comparison of Figure 5a with the stretching field displayed in Figure 3a indicates that the manifolds indeed produce regions of high stretching (red and yellow). However, the manifolds of this point fail to predict the structure of the highly segregated red regions near the walls, and bears *no resemblance whatsoever with the structure of the regions with the highest stretching*, displayed in Figure 4a. Instead, these high stretching regions are in excellent agreement with the structure of the unstable manifolds, shown in Figure 5b, of a pair of period-2 hyperbolic points located on the horizontal axis at $x=0.0605$ and $x=0.9791$.

Three period-1 hyperbolic points were found for $T=7.0$. At $t=0$, these points are on the horizontal axis at (i) $x=0.0601$ (hyperbolic), (ii) $x=0.3405$ (elliptic, center of the large island), and (iii) $x=0.8621$ (also hyperbolic). The positions after eight periods of particles initially placed in the neighborhood of points i and iii are displayed in Figures 5c and 5d, respectively. Comparison of Figures 5c and 5d with the stretching field in Figure 3c shows that branches of the unstable manifolds of both points correspond to high stretching (red and yellow) regions. However, only the manifold of point i gives a good prediction of the location of points with the highest stretching values, which are displayed in Figure 4b. Similarly to the period-1 point for $T=5.6$, in the short time considered here the manifolds of point iii fail to approach the highest stretching regions near the walls or around the island.

Finally, three period-1 points were found for $T=9.0$. At $t=0$, these points are on the horizontal axis at (i) $x=0.03785$ (hyperbolic), (ii) $x=0.4893$ (elliptic, center of the island), and (iii) $x=0.8905$ (hyperbolic). The unstable manifolds of points i and iii (as revealed by particles that are initially located close to the points and are convected by the flow for six periods) are shown in Figures 5e and 5f, respectively. At first glance, these figures look very similar. In both cases the main feature is that the manifolds do not approach the large island at the center of the cavity (this is important and will be discussed later). However, careful examination and comparison with Figures 3d (stretching field) and 4c (highest stretching points) shows that the manifolds of point i predict the structure of high stretching regions considerably better than those of point iii.

The reason for the various degrees of agreement between stretching and manifolds is that unstable manifolds may not be the only source of high stretching in the cavity flow. Although manifolds are clearly important, other characteristics of the flow also have a role in controlling stretching of material elements. As mentioned in the introduction, singular points located at the corners of the flow impose extremely high stretching in their environs. Points passing close to these singularities will accumulate stretching at a very high rate. Figures 6a–6c show the final locations after several periods of a large number of tracers that were initially placed very close to the

corners. Comparisons between Figures 4a and 6a ($T=5.6$), Figures 4b and 6b ($T=7.0$), and Figures 4c and 6c ($T=9.0$) clearly show that the corner singularities have a major impact in determining the structure of the high stretching regions. Manifolds still play an important role: because of the highly correlated, time-invariant structure of the manifolds, a point that passes close to a corner and that also belongs to the manifold has a large probability of returning to the neighborhood of the corner a short time later. Manifolds from the period-2 points for $T=5.6$ and from points denoted by i for $T=7.0$ and $T=9.0$ pass close to the corners and efficiently predict the structure of the regions with the highest stretching values. Manifolds from the only period-1 point for $T=5.6$ and from points denoted by iii for $T=7.0$ and $T=9.0$ do not approach the corners for short times, and fail to predict the structure of the highest stretching regions in the early stages of the process. Although it is also possible that hyperbolic points could exist in the neighborhood of the corners and play a role in the formation of the structures displayed in Figures 6a-6c, this hypothesis is difficult to investigate due to limited numerical resolution that can be achieved in the neighborhood of corners due to the presence of singularities at the corners. One might wonder, however, whether the corners themselves could have manifolds. In some sense, the moving wall itself is an outgoing eigendirection for the corners (a vector pointing in this direction preserves orientation), with the associated "manifold" starting from one corner and ending in the opposite one. However, this is a trivial case, since this "manifold" does not penetrate the flow domain.

The separate roles of corners and unstable manifolds of periodic points are further illustrated in Figures 7a and 7b. Figure 7a displays the stretching field for an *aperiodic* cavity flow generated using a symmetry-breaking prescription (Franjione et al., 1989). Since the flow is no longer periodic, it does not have periodic points. However, segregated high stretching regions, generated by the corner singularities, are still present, demonstrating that such regions can exist in the absence of unstable manifolds of hyperbolic periodic points. While it is also possible that the segregated high stretching regions in Figure 7a could be generated by manifolds of an invariant hyperbolic set located very close to the walls and associated to the corner singularities, it is not clear how the existence of such an invariant structure could be ascertained given the limited numerical resolution that can be achieved in the neighborhood of corners.

On the other hand, it is easy to show that the corner singularities play a major role in the formation of the segregated high stretching region. Figure 7b shows the stretching field generated using a modified, highly idealized cavity flow that has no singular corner points. To remove the singularities, the velocity along the moving walls is no longer constant and is redefined as $V_x=(\pi/2)U\cos(\pi x)$. The results displayed in Figure 7b correspond to a periodic flow with $T=7.0$. High stretching regions near walls have now disappeared, high stretching points are considerably less segregated than in previous cases, and their locations are accurately predicted by the manifolds, shown in Figure 7c, of a period-1 hyperbolic point which at $t=0$ is located at $x=0.0675$ on the horizontal axis. Moreover, as it is apparent in the figure, in the short time scale of this computation, the manifolds do not approach the corners of the cavity. High stretching regions fail to develop near the boundaries of the cavity, and in this case *low stretching regions* are observed near the static vertical walls.

Low stretching regions

The spatial distribution of low stretching points also has significant implications for mixing and deserves further examination. For flows with large islands, most of the low stretching points will be located inside the islands. Both for $T=7.0$ (Figure 3c) and for $T=9.0$ (Figure 3d) the stretching field inside the large regular islands is highly structured. Points with the lowest stretchings (black) are located in a large core with complicated shape situated at the center of the island. In addition, low stretching points also concentrate on small segregated regions near the rim of the large islands. Figure 3c shows two such regions to the left and another to the right of the large island. Similarly, Figure 3d shows a chain of seven low stretching regions surrounding the large island at the center of the flow field. In all likelihood, these regions are generated by chains of small regular islets that surround the main island, and are separated from it by a thin chaotic layer. This hypothesis is hard to verify given the limited numerical resolution available.

The structure of low stretching regions outside islands also depends strongly on T. Figure 8a shows those regions for $T=5.6$, 20 periods. For this globally chaotic condition, the points are scattered throughout the chaotic region in a roughly uniform fashion. On the other hand, for flows that have large islands, particle trajectories passing close to islands tend to stick to the islands for long times. As a result, low stretching points are expected to populate both the interior and the neighborhood of islands (Grassberger et al., 1988; Sepulveda et al., 1989; Horita et al., 1990; Muzzio et al., 1991a, 1992a,b; Shlesinger et al., 1993). As mentioned above, this is indeed the case for $T=9.0$, where low stretching points not only populate the island but also concentrate in a sharply defined spiral structure with several major arms wrapped around the island (Figure 8b). Indirect supporting evidence can be inferred from the previous case; for $T=5.6$, the flow has no large islands, and a fairly uniform spatial distribution of low stretching points is obtained (Figure 8a).

However, this "sticking process" is not universal. Figure 8c shows the location of low stretching points for $T=7.0$, 20 periods. The points are restricted inside the islands, except for a few points that populate the chaotic region sparsely and do not accumulate nearby islands. This major difference in behavior between this case and the case corresponding to $T=9.0$ is also related to the unstable manifolds of periodic points. As it is shown in Figure 5c for $T=7.0$, the unstable manifolds of point i tightly surround the largest island in the system, preventing low stretching orbits from sticking to the island and destroying the low stretching regions observed nearby islands in other flows (Sepulveda et al., 1989; Horta et al., 1990; Muzzio et al., 1991a, 1992a,b). To the best of our knowledge, such a case has not been observed for other flows, and low stretching chaotic regions are always expected to accumulate in the neighborhood of islands. As the case for $T=7.0$ shows, there are exceptions to this "rule."

Statistical Analysis of the Stretching Field

The statements made in the previous section concerning the

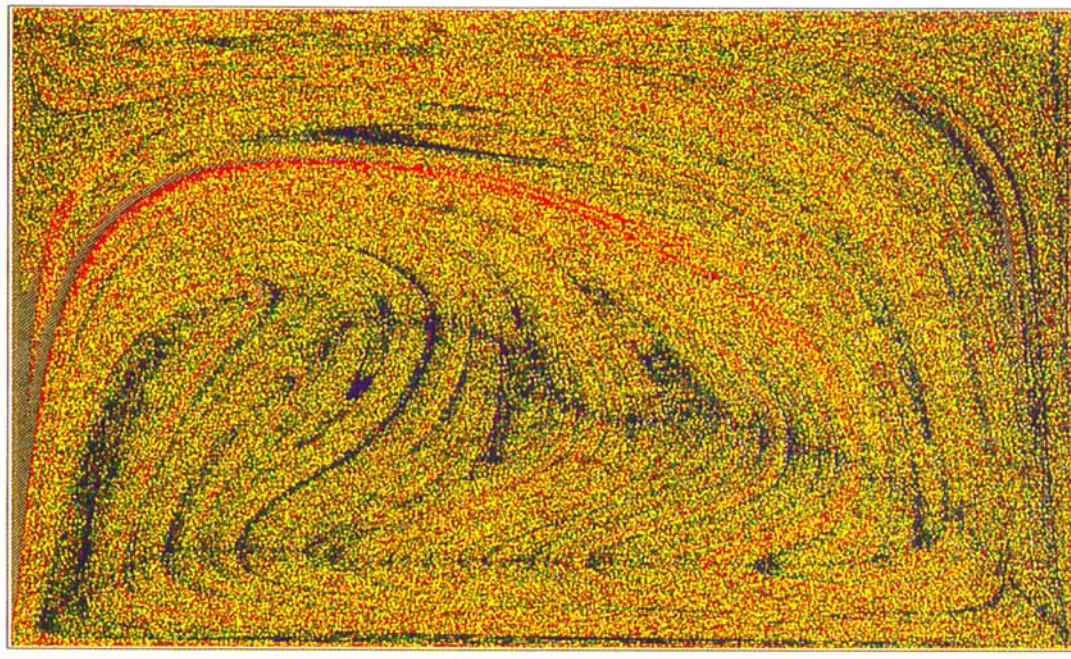

(a)

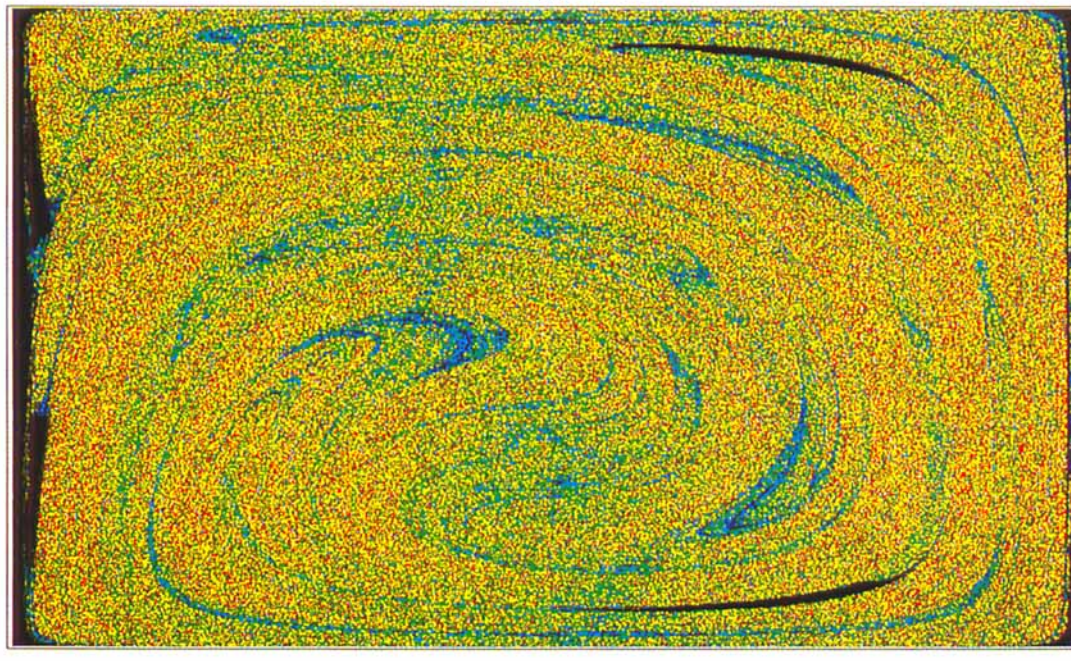

(b)

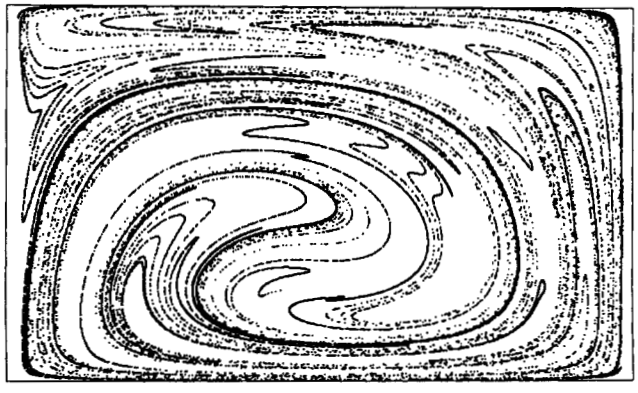

(c)

Figure 7. (a) Stretching field of aperiodic cavity flow generated using symmetry breaking procedure.

Average period is $T = 7.0$. Similarly to Figure 3, points are color-coded according to intensity of stretching; blue corresponds to $\log\lambda < 6.9$, green to $6.9 < \log\lambda < 8.5$, yellow to $8.5 < \log\lambda < 10.0$, and red to $10.0 < \log\lambda$.

Figure 7. (b) Stretching field corresponding to modified periodic cavity flow without corner singularities, $T = 7.0$.

Black corresponds to $\log\lambda < 3.5$; dark blue to $3.5 < \log\lambda < 6.3$, light blue to $6.3 < \log\lambda < 10.0$, green to $10.0 < \log\lambda < 12.0$, yellow to $12.0 < \log\lambda < 14.0$, and red to $14.0 < \log\lambda$.

Figure 7. (c) Unstable manifolds of period-1 hyperbolic point initially located at $x = 0.0675$.

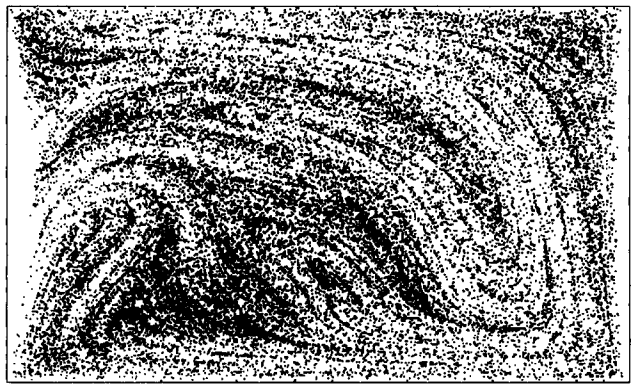

(a)

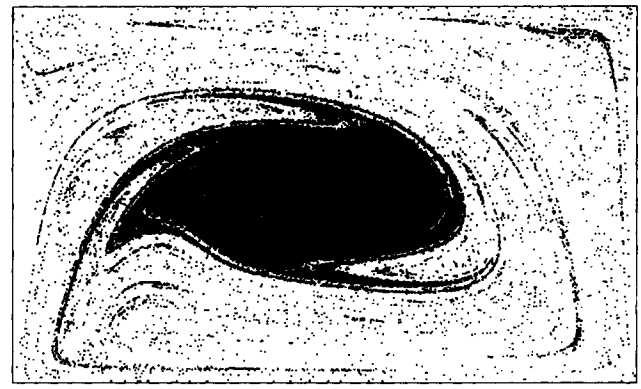

(b)

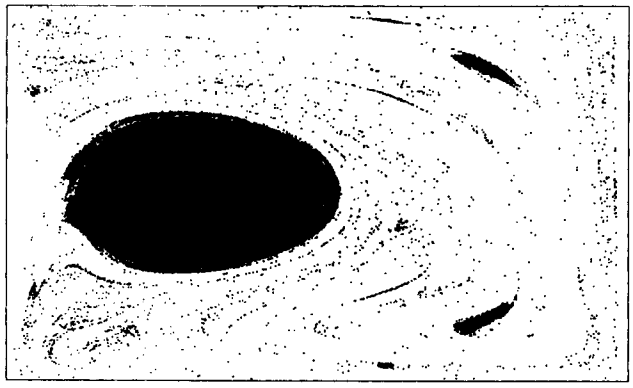

(c)

Figure 8. Spatial distribution of particles with low stretching intensities after *n* periods.

Total number of particles in these computations is 365,820. (a) $T=5.6$, $n=20$, 32,317 particles, $\log(\lambda)<5.6$; (b) $T=9.0$, $n=12$, 67,579 particles, $\log(\lambda)<3.9$; (c) $T=7.0$, $n=20$, 57,477 particles, $\log(\lambda)<3.3$.

effects of unstable manifolds, islands, and corner singularities on the structure of the stretching field are mostly qualitative. In this section, statistical calculations are used to demonstrate quantitatively the role of manifolds in preventing the formation of low stretching regions in the neighborhood of islands for $T=7.0$, and the role of corner singularities in generating segregated high stretching regions.

As was mentioned in the second section, a number of recent studies have focused on the statistics of the stretching process in chaotic flows, both in terms of short-time Lyapunov exponents and of stretching of material elements. Since in chaotic systems the stretching λ increases exponentially with time, the fluctuations of λ are best described by computing $H_n(\log\lambda)$, the probability density function of $\log\lambda$ (logarithms of base 10 are used throughout this section). $H_n(\log\lambda)=dN(\log\lambda)/d(\log\lambda)$ is obtained from simulations similar to those used to generate Figure 3 by counting the number of points $dN(\log\lambda)$ that have stretching values in the range of $[\log\lambda, \log\lambda+d(\log\lambda)]$. Since in average the local striation thickness is inversely proportional to the stretching, $H_n(\log\lambda)$ can be conceptually interpreted as a spectrum of intensities of the fluid mechanical mixing process. In order to assess the effect of islands on the statistics of the stretching field, $H_n(\log\lambda)$ is computed using two types of initial conditions (IC):

IC 1: For simulations that include both chaotic and nonchaotic (regular) regions, the particles are placed on a uniform array spanning the entire flow domain.

IC 2: For simulations that consider only chaotic regions, the particles are initially placed in a small array within the chaotic region, and are scattered throughout this region by stirring them with the flow for 20 periods before computing their stretching values.

Figure 9a shows $H_n(\log\lambda)$ computed for $T=5.6$ using 25,600 particles, initially distributed uniformly throughout the entire flow (IC 1). The figure shows $H_n(\log\lambda)$ computed for 20 periods at intervals of two periods. As n increases, points accumulate stretching and the curves shift to the right. After a few periods of transition, the central part of each curve develops a bell shape similar to those reported for other chaotic flows for spectra of Lyapunov exponents (Grassberger et al., 1988; Sepulveda et al., 1989; Horita et al., 1990; Városi et al., 1991; Pierrehumbert, 1991; Beigie et al., 1993) or stretching distributions (Muzzio et al., 1991a, 1992a,b). The most striking feature of this figure, however, is the presence of a very long tail on the high stretching end of each curve, revealing extremely high stretchings experienced by some particles. These tails are generated by the segregated high stretching regions (red points) in Figure 3a. After 20 periods, the largest stretching values have a magnitude of $O(10^{30})$. The tail is more clearly observed in the insert, which displays $\log(H_n)$ vs. $\log\lambda$ for $n=20$.

Figure 9b shows $H_n(\log\lambda)$ for $T=7.0$ for particles initially located throughout the entire flow domain (IC 1). The curves show $H_n(\log\lambda)$ calculated every two periods for $n=2$–20, and the insert shows $H_n(\log\lambda)$ for $n=20$. Once again, a long tail is present for high values of λ, corresponding to segregated particles that move along the unstable manifolds and experience very high stretchings. In addition, each curve has two

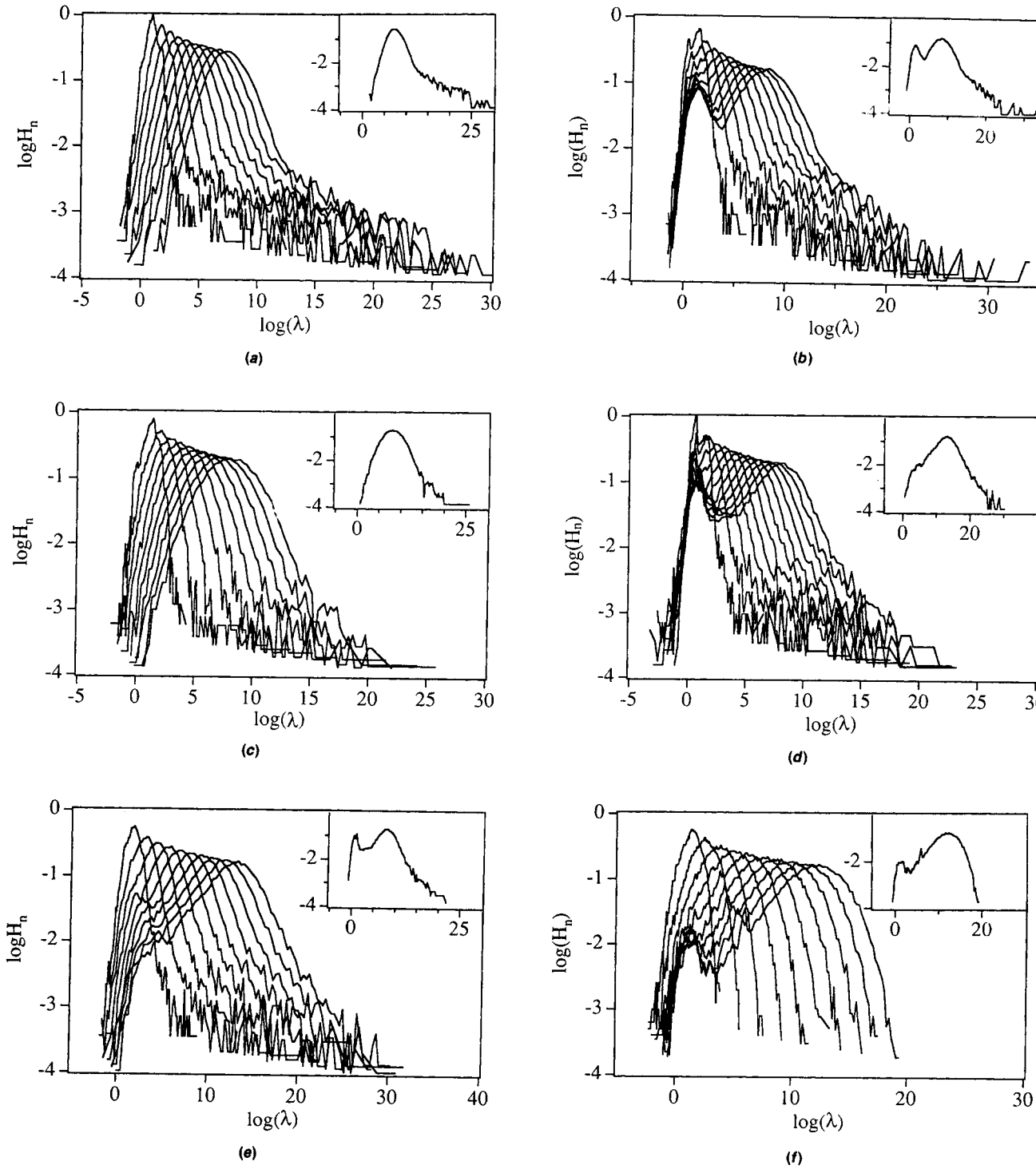

Figure 9. $H_n(\log\lambda)$ for cavity flow, for (a) $T = 5.6$, 2 to 20 periods; (b) $T = 7.0$, 2 to 20 periods; (c) $T = 7.0$, 2 to 20 periods; (d) $T = 9.0$, 1 to 12 periods; (e) $T = 9.0$, 3 to 12 periods; (f) $T = 7.0$, 2 to 20 periods (modified cavity flow without corner singularities).

Figures 9a, 9b, 9d, and 9f were obtained for particles initially placed throughout entire flow region. Figures 9c and 9e contain particles initially placed in small array inside chaotic region and scattered throughout chaotic region using 20 flow periods. In all cases, insert shows $H_n(\log\lambda)$ at end of last period.

peaks, indicating a situation more complex than was observed in Figure 9a. While the peak to the right is bell-shaped and corresponds to the chaotic region, the peak to the left is produced by the regular island and is characterized by the presence of multiple subpeaks. As n increases, the peak associated with the chaotic region moves to the right at a uniform rate, indicating the exponential stretching of the particles in the chaotic region. On the other hand, the peak corresponding to the

regular region hardly moves at all. Figure 9c shows $H_n(\log\lambda)$ for $T=7.0$, 20 periods, for particles populating *only the chaotic region* (IC 2). The peak associated with the regular island has completely disappeared, and the curves look identical to those shown in Figure 9a for the case without islands. This indicates that for $T=7.0$, the stretching process in the chaotic region is largely independent of the presence of islands. This is due to the structure of the unstable manifold discussed in the previous section, which has branches wrapped around the island, effectively cutting off the island from the chaotic region.

Figure 9d shows $H_n(\log\lambda)$ computed for $T=9.0$ with particles initially covering the entire flow domain (IC 1). The curves correspond to $n=3$–12. Again, the curves display two peaks and a very broad range of values of λ. At a first glance, the curves in Figure 9d look very similar to those in Figure 9b. However, for this case, the high stretching tail is considerably shorter, in correspondence with the "looser" structure of the high stretching region observed in Figures 3d and 4c. As discussed above, for this case the island has a strong effect on the stretching experienced by particles *inside* the chaotic region. Figure 9e shows $H_n(\log\lambda)$ for $T=9.0$ for particles only in the chaotic region (IC 2). The low stretching branch of each curve displays a considerable amount of distortion when compared with the curves corresponding to the case without islands (Figure 9a); low stretching points occur with higher frequency. In general, these distortions are to be expected, because as mentioned above, regions of low stretching tend to develop in the neighborhood of islands. However, this "rule" lacks general validity; for $T=7.0$, the unstable manifolds are tightly wrapped around the island, low stretching regions are prevented from developing, and $H_n(\log\lambda)$ for the chaotic region is essentially identical to that one corresponding to a case without large islands.

The role played by corner singularities on the formation of segregated high stretching regions can be quantitatively investigated using statistical computations. An immediate approach is to compare the results presented in Figures 9a–9e with similar calculations for flows that lack singularities. Figure 9f shows $H_n(\log\lambda)$ for the modified cavity without singularities, $T=7.0$, with particles initially located throughout the entire flow domain (IC 1). The curves correspond to $n=2$–20, and the insert shows $H_n(\log\lambda)$ for $n=20$. For this condition, the flow has two small islands, which are revealed by the peak to the left of each curve. The most important feature of the curves in Figure 9f, however, is the absence of the high stretching tails; compare Figure 9f with Figures 9a–9e. Although the modified cavity has hyperbolic periodic points with unstable manifolds, in the absence of corner singularities these manifolds do not generate the segregated high stretching regions observed nearby walls for the physically realizable cavity flow, and as a result, the spectra $H_n(\log\lambda)$ are devoid of high stretching tails. The lack of high stretching tails exhibited by the curves in Figure 9f is in qualitative agreement with observations for several other flows which also lack singularities (Muzzio et al., 1991a, 1992a,b), and clearly indicates to a distinctive role of the corner singularities in creating the segregated high stretching regions and the high stretching tails.

Conclusions

This article focuses on the structure of the stretching field in time-periodic chaotic cavity flows. The evolution of this field is dominated by regular islands, singular corners, and unstable manifolds of hyperbolic points. The combined effects of manifolds and corner singularities is one of the main differences between the cavity flow and the flow between eccentric cylinders, which is the only other physically realizable flow for which the stretching field has been investigated. The flow between eccentric cylinders has no singularities, and the formation of high stretching regions could be analyzed by focusing exclusively on manifolds. On the other hand, in the cavity flow, regions of high stretching coincide with branches of the unstable manifolds of hyperbolic points only in cases where those manifolds approach the singular corners. This role of corners has important implications for mixing in cavity flows. High rates of stretching correspond to fast production of intermaterial area, hence, efficient micromixing. However, for cavities with corner singularities these high stretching regions are highly segregated and therefore they are poorly mixed in a global sense. The role of corners is further confirmed using statistical analysis. For the cavity with corner singularities, the probability density function of stretching shows long high stretching tails; for a modified cavity flow without singularities, the tails are no longer observed. Since manifolds are invariant curves of infinite length and particles passing close to either periodic points or corners should eventually visit every position within the chaotic region, the persistence of these effects for long times remains an open question that we plan to address in future research efforts.

Low stretching (poor mixing) regions are found within regular islands. In some cases, low stretching regions spread out of the islands and into the chaotic regions, and for such cases the probability function of stretching shows distortions in the low stretching region. However, as it is demonstrated here, such effects are not universal, and depend on the details of the structure of the islands and that of the unstable manifolds; an example is shown where manifolds pass close to the islands, preventing the formation of segregated low stretching subregions within the chaotic region. For such cases, the probability density function of stretching in the chaotic region is qualitatively identical to that of a flow without islands.

The stretching field can affect the dynamics of other processes in the flow. An example is mixing of particles with finite size and mass, which has a wide range of applications in science and engineering. Discrete particles are subject to several dissipative forces and their motion is not Hamiltonian. Discrete particles in chaotic flows organize themselves in nontrivial spatial structures; depending on the values of system parameters, the fraction of system volume occupied by finite particles may increase or decrease with time. The size and structure of the region of the flow populated by particles depends on the stretching field of the underlying Hamiltonian flow. Such results were not discussed here for the sake of brevity and coherence of presentation; a full description of the discrete particle mixing for a variety of flow conditions will be communicated in a separate article (see also Liu and Peskin, 1993).

Acknowledgments

This work was supported by grants from the Exxon Foundation, the Merck Foundation, and Rutgers' CAIP center to FJM, by NSF grant ECS 9110424 to RLP, and by a grant from the Electric Power Research Institute to RLP. Dr. Sandra Walther at CAIP developed

the scientific data management and visualization tools used in the research.

Notation

L = flow length scale, defined as the length of a moving wall in the cavity
l = vector used to compute stretching
l_0 = initial condition for vector l
p = pressure field
Re = Reynolds number
T = dimensionless flow period
U = flow velocity scale, defined as the velocity of a moving wall in the cavity
v = velocity field
x = vector giving the coordinates of l
X_0 = vector giving the coordinates of l_0

Greek letters

λ = stretching experienced by vector l
μ = fluid viscosity
ρ = fluid density

Literature Cited

Aref, H., "Stirring by Chaotic Advection," *J. Fluid Mech.*, **143**, 1 (1984)

Aref, H., and S. Balachandar, "Chaotic Advection in a Stokes Flow," *Phys. Fluids*, **29**, 3515 (1986).

Aref, H., and S. W. Jones, "Enhanced Separation of Diffusing Particles by Chaotic Advection," *Phys. Fluids A*, **1**, 470 (1988).

Beigie, D., A. Leonard, and S. Wiggins, "A Global Study of Enhanced Stretching and Diffusion in Chaotic Tangles," *Phys. Fluids A*, **3**, 1039 (1991).

Beigie, D., A. Leonard, and S. Wiggins, "Statistical Relaxation under Non-Turbulent Chaotic Flows: Non-Gaussian High Stretch Tails of Finite-Time Lyapunov Exponent Distributions," *Phys. Rev. Lett.*, **70**, 275 (1993).

Chaiken, J., R. Chevray, M. Tabor, and Q. M. Tan, "Experimental Study of Lagrangian Turbulence in a Stokes Flow," *Proc. Roy. Soc. Lond.*, **A408**, 165 (1986).

Chien, W. L., H. Rising, and J. M. Ottino, "Laminar and Chaotic Mixing in Cavity Flows," *J. Fluid Mech.*, **170**, 355 (1986).

Dahm, W., K. B. Southerland, and K. A. Buch, "Direct, High Resolution Measurements of the Fine Scale Structure of $Sc \gg 1$ Molecular Mixing in Turbulent Flows," *Phys. Fluids A*, **3**, 1115 (1991).

Franjione, J. G., C. W. Leong, and J. M. Ottino, "Symmetries Within Chaos: a Route to Effective Mixing," *Phys. Fluids A*, **1**, 1172 (1989).

Grassberger, P., R. Badii, and A. Politi, "Scaling Laws for Invariant Measures on Hyperbolic and Nonhyperbolic Attractors," *J. Statist. Phys.*, **51**, 135 (1988).

Horita, T., H. Hata, and H. Mori, "Long-Time Correlations and Expansion-Rate Spectra of Chaos in Hamiltonian Systems," *Prog. Theor. Phys.*, **83**, 1065 (1990).

Jones, S. W., "The Enhancement of Mixing by Chaotic Advection," *Phys. Fluids A*, **3**, 1081 (1991).

Khakhar, D. V., H. Rising, and J. M. Ottino, "Analysis of Chaotic Mixing in Two Model Systems," *J. Fluid Mech.*, **172**, 419 (1986).

Leong, C. W., and J. M. Ottino, "Experiments on Mixing Due to Chaotic Advection in a Cavity," *J. Fluid Mech.*, **209**, 463 (1989).

Leong, C. W., "Chaotic Mixing of Viscous Fluids in Time-Periodic Cavity Flows," PhD Dissertation, University of Massachusetts (1990).

Liu, M., "Numerical Study of Nonlinear Dynamics of Particles and Chaotic Mixing in Two Dimensional Periodic Driven Cavity Flows," PhD dissertation, Rutgers, State University of New Jersey (1992).

Liu, M., and R. L. Peskin, "Chaos and Mixing of Particles in 2D Periodic Chaotic Flows," *5th Int. Symp. on Gas-Solid Flows*, ASME **166**, 95 (1993).

Muzzio, F. J., and J. M. Ottino, "Evolution of a Lamellar System with Diffusion and Reaction: a Scaling Approach," *Phys. Rev. Lett.*, **63**, 47 (1989a).

Muzzio, F. J., and J. M. Ottino, "Dynamics of a Lamellar System with Diffusion and Reaction: Scaling Analysis and Global Kinetics," *Phys. Rev. A*, **40**, 7182 (1989b).

Muzzio, F. J., and J. M. Ottino, "Diffusion and Reaction in a Lamellar System: Self-Similarity with Finite Rates of Reaction," *Phys. Rev. A.*, **42**, 5873 (1990).

Muzzio, F. J., P. D. Swanson, and J. M. Ottino, "The Statistics of Stretching and Stirring in Chaotic Flows," *Phys. Fluids A*, **3**, 822 (1991a).

Muzzio, F. J., M. Tjahjadi, and J. M. Ottino, "Self-Similar Drop-Size Distributions Produced by Breakup in Chaotic Flows," *Phys. Rev. Lett.*, **67**, 54 (1991b).

Muzzio, F. J., C. Meneveau, P. D. Swanson, and J. M. Ottino, "Scaling and Multifractal Techniques for Analysis of Mixing in Chaotic Flows," *Phys. Fluids A*, **4**, 1439 (1992a).

Muzzio, F. J., P. D. Swanson, and J. M. Ottino, "Mixing Distributions Produced by Multiplicative Stretching in Chaotic Flows," *Int. J. Bifurc. Chaos*, **2**, 37 (1992b).

Ottino, J. M., "Description of Mixing with Diffusion and Reaction in Terms of the Concept of Material Surfaces," *J. Fluid Mech.*, **114**, 83 (1982).

Ottino, J. M., C. W. Leong, H. Rising, and P. D. Swanson, "Morphological Structures Produced by Mixing in Chaotic Flows," *Nature*, **333**, 419 (1988).

Pierrehumbert, R. T., "Large Scale Horizontal Mixing in Planetary Atmosphere," *Phys. Fluids A*, **3**, 1250 (1991).

Rom-Kedar, V., A. Leonard, and S. Wiggins, "An Analytical Study of Transport, Mixing and Chaos in an Unsteady Vortical Flow," *J. Fluid Mech.*, **214**, 347 (1990).

Sepulveda, M. A., R. Badii, and E. Pollak, "Spectral Analysis of Conservative Dynamical Systems," *Phys. Rev. Lett.*, **63**, 1226 (1989).

Shlesinger, M. F., G. M. Zaslavsky, and J. Klafter, "Strange Kinetics," *Nature*, **363**, 31 (May 6, 1993).

Swanson, P. D., and J. M. Ottino, "A Comparative Computational and Experimental Study of Chaotic Mixing of Viscous Fluids," *J. Fluid Mech.*, **213**, 227 (1990).

Tjahjadi, M., H. A. Stone, and J. M. Ottino, "Satellite and Subsatellite Formation in Capillary Breakup," *J. Fluid Mech.*, **243**, 297 (1992).

Városi, F., T. M. Antonsen, and E. Ott, "The Spectrum of Fractal Dimensions of Passively Convected Scalar Gradients in Chaotic Fluid Flows," *Phys. Fluids A*, **3**, 1017 (1991).

Wiggins, S., *Chaotic Transport in Dynamical Systems*, Springer-Verlag, New York (1992).

Manuscript received June 21, 1993, and revision received Oct. 4, 1993.